

# PanoSSC: Exploring Monocular Panoptic 3D Scene Reconstruction for Autonomous Driving

Yining Shi<sup>1,3\*</sup>, Jiusi Li<sup>1\*</sup>, Kun Jiang<sup>1†</sup>, Ke Wang<sup>2</sup>, Yunlong Wang<sup>1</sup>, Mengmeng Yang<sup>1</sup>, Diange Yang<sup>1†</sup>  
<sup>1</sup> School of Vehicle and Mobility, Tsinghua University, <sup>2</sup> Kargobot <sup>3</sup> DiDi Chuxing

## Abstract

Vision-centric occupancy networks, which represent the surrounding environment with uniform voxels with semantics, have become a new trend for safe driving of camera-only autonomous driving perception systems, as they are able to detect obstacles regardless of their shape and occlusion. Modern occupancy networks mainly focus on reconstructing visible voxels from object surfaces with voxel-wise semantic prediction. Usually, they suffer from inconsistent predictions of one object and mixed predictions for adjacent objects. These confusions may harm the safety of downstream planning modules. To this end, we investigate panoptic segmentation on 3D voxel scenarios and propose an instance-aware occupancy network, PanoSSC. We predict foreground objects and backgrounds separately and merge both in post-processing. For foreground instance grouping, we propose a novel 3D instance mask decoder that can efficiently extract individual objects. We unify geometric reconstruction, 3D semantic segmentation, and 3D instance segmentation into PanoSSC framework and propose new metrics for evaluating panoptic voxels. Extensive experiments show that our method achieves competitive results on SemanticKITTI semantic scene completion benchmark.

## 1. Introduction

Accurate understanding of the 3D surroundings is an essential prerequisite for safe autonomous driving systems. Apart from the mature object-centric perception pipelines which consist of detection, tracking and prediction [27], the newly emerging occupancy networks cast new insights for fine-grained scene understanding [35, 38]. Occupancy

<sup>†</sup>This work was done during Yining Shi’s internship at DiDi Chuxing. \*: Yining Shi and Jiusi Li contributed equally to this work. †: Corresponding authors: Kun Jiang, Diange Yang (jiangkun@mail.tsinghua.edu.cn, ydg@mail.tsinghua.edu.cn).

This work was supported in part by the National Natural Science Foundation of China under Grants (U22A20104, 52372414, 52102464). This work was also sponsored by Tsinghua University-DiDi Joint Research Center for Future Mobility.

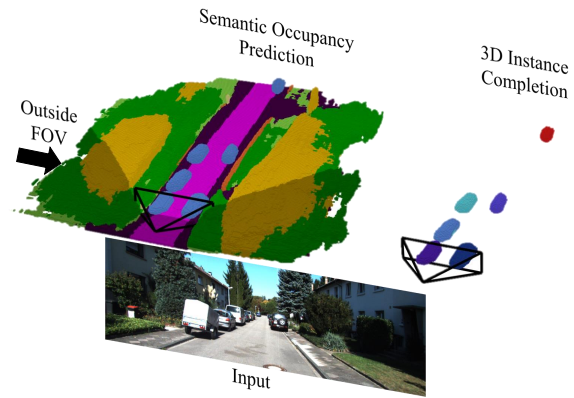


Figure 1. Panoptic 3D scene reconstruction from a monocular RGB image for outdoor scenes with PanoSSC. Our method infers voxel-level occupancy, semantics and instance ids.

networks are more capable of representing partly occluded, deformable, or semantically not well-defined obstacles and conducting open-world general object detection, so recently they are widely investigated in both academia and industry.

Reconstructing the surroundings as 3D voxels originates from semantic scene completion (SSC) from a single LiDAR frame. Since Tesla announced its vision-only occupancy network, various vision-centric occupancy networks [11, 39, 42] are proposed with additional voxel-level labels and occupancy prediction benchmarks on nuScenes, KITTI360, and Waymo open dataset [19, 38, 39, 42].

Although recent vision-based methods perform as well as LiDAR-based methods on segmentation task [11, 39], **instances extraction** in semantic mapping are less explored. Understanding instances in the environment is able to eliminate inconsistent semantic predictions of one object and mixed predictions for adjacent objects, while these confusions may harm the safety of downstream planning modules. We intend to conduct instance-aware semantic occupancy prediction on SSC benchmarks since SSC tasks require an entire representation of a single object. A concurrent work, PanoOcc [30, 43], conducts panoptic segmentation on LiDAR panoptic benchmark via multi-task learning

of occupancy prediction and object detection. The main difference between this paper and PanoOcc [43] lies in that we don't assume labeling objects as bounding boxes and only learn instances with segmentation labels. Hence, we are motivated to adapt to diverse environments with obstacles in which bounding boxes do not fit.

We propose PanoSSC, a novel monocular panoptic 3D scene reconstruction method. PanoSSC consists of image encoder, 2D to 3D transformer, semantic occupancy head and transformer-based mask decoder head. Image features are lifted to 3D space for 3D semantic occupancy prediction and 3D instance completion. Unlike previous semantic occupancy networks that adopt a per-voxel classification formulation, we design a 3D mask decoder for foreground instance completion and perform mask-wise classification. This design is motivated by an insight: semantic segmentation and instance segmentation for 2D images can benefit from multi-task learning [12, 13]. Similar to [22], we propose a strategy for merging results of the two heads to obtain voxel-level occupancy, semantics and instance ids. An graphical illustration is shown in Fig. 1.

In summary, our main contributions are listed as follows:

1. We propose the task of panoptic 3D scene reconstruction for outdoor scenes, aiming to predict voxel-level occupancy, semantics and instance id.
2. We propose a novel monocular semantic occupancy network, PanoSSC, which includes two prediction heads to perform semantic occupancy prediction and 3D instance completion respectively. The joint learning of these two heads can promote each other.
3. Our method achieves competitive semantic occupancy prediction results compared to the monocular pioneering work on SemanticKITTI [1]. It is also the first to tackle panoptic 3D semantic scene reconstruction on outdoor.

## 2. Related works

**Semantic occupancy prediction.** Semantic occupancy prediction, originally called semantic scene completion (SSC), is introduced in SSCNet [36] for indoor scenes, which aims to jointly address 3D semantic segmentation and 3D scene completion and achieve mutual promotion. Since then, many SSC methods on indoor have been proposed, which directly use depth images [17, 18] from RGB-D as input or encode depth information as occupancy grids [8, 45] or TSDF [4, 36, 48]. SemanticKITTI [1] is the first large-scale dataset that proposes this task for LiDAR in the real outdoor world. Most methods [6, 32, 34, 44, 46] for outdoor depend on LiDAR point clouds. After Tesla's Occupancy Network, semantic occupancy prediction based on low-cost cameras has received extensive attention. MonoScene [2] is the first to infer dense 3D voxelized semantic scenes from a single RGB image. OccDepth [28] further uses implicit depth information from stereo images for 3D struc-

ture reconstruction. To avoid the ambiguity of 3D features caused by occlusion, VoxFormer [20] first forms sparse 3D voxel features of the visible area and then densifies them. TPVFormer [11] proposes an efficient tri-perspective view representation to replace voxel-based features and generates occupancy prediction with multi-view images. Our method is able to perform semantic occupancy prediction from a monocular image, and further distinguish different instances belonging to the same foreground category.

**Semantic and panoptic segmentation.** Semantic and panoptic segmentation are thoroughly investigated with the development of deep learning. Since FCNs [25], semantic segmentation mainly relies on per-pixel classification, while mask classification dominates for instance-level segmentation tasks [9, 14]. In 2D domain, early mask-based methods [3, 10] first predict bounding boxes and then generate a binary mask for each box, while others [5, 22, 41] discard the boxes and directly predict masks and categories. In the automotive perception domain, vision bird's eye view (BEV) algorithms [21, 24, 31] focus on the transformation from perspective view (PV) to BEV and segment drivable areas, lanes and vehicles on BEV. 3D panoptic segmentation are designed for sparse LiDAR point clouds [47]. Dahnert et al. [7] unify the tasks of geometric reconstruction, 3D semantic segmentation, and 3D instance segmentation into panoptic 3D scene reconstruction for indoor scenes, and propose a monocular method. PNF [16] generates panoptic neural scene representation with self-supervision from an RGB sequence, while it focuses on offline reconstruction like most other NeRF-style methods rather than real-time semantic occupancy prediction. We address outdoor panoptic 3D scene reconstruction and generate 3D voxel binary mask for each object to conduct mask classification and instance-aware semantic occupancy prediction.

**Multi-task learning.** For images, many works [12, 13] regard semantic segmentation and instance segmentation as related tasks for joint learning and achieve good performance. For autonomous driving, multi-task learning is widely used in LiDAR semantic segmentation. LidarMultiNet [47] is a unified framework for 3D semantic segmentation, object detection and panoptic segmentation. JS3CNet [46] exploits the shape priors from semantic scene completion to improve the performance of segmentation. Inspired by these works, we design two heads for semantic occupancy prediction and 3D instance completion respectively, and conduct joint learning to achieve mutual promotion.

## 3. Methodology

### 3.1. Architecture

Semantic occupancy prediction is to discretize 3D scene into voxels and assign each voxel a semantic label  $C = \{c_0, c_1, \dots, c_N\}$ , where  $c_0$  denotes free class and  $N$  is the

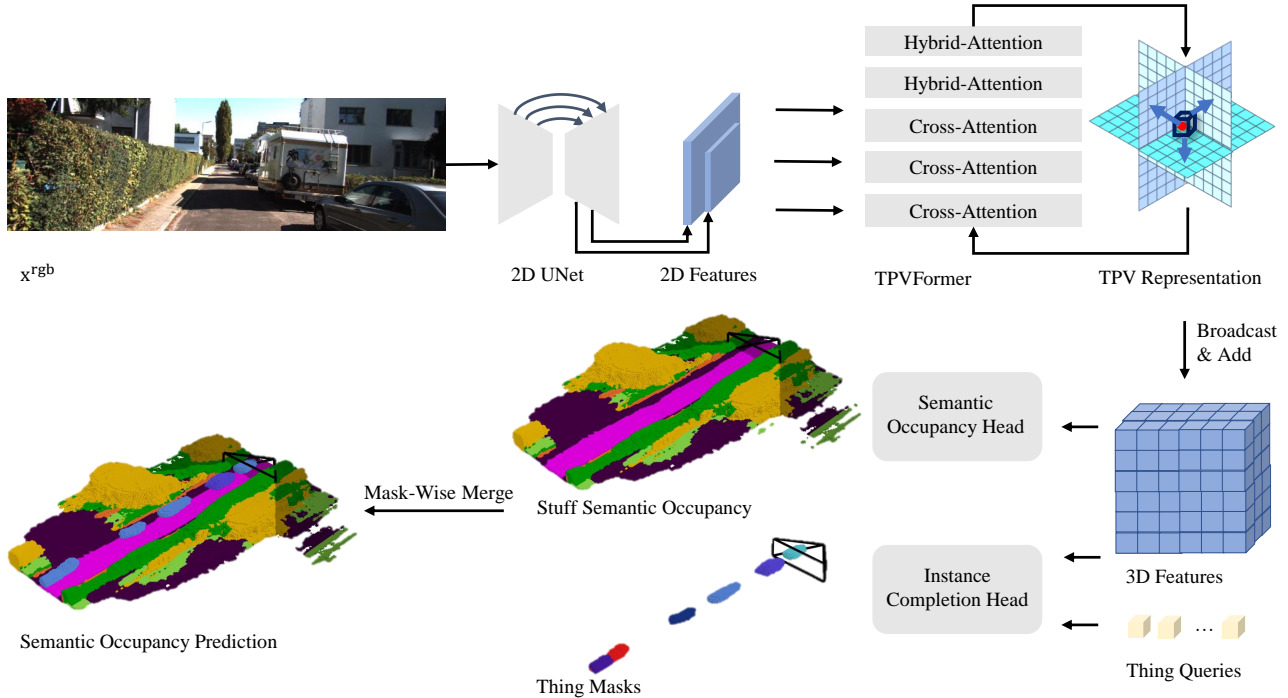


Figure 2. PanoSSC framework. We adopt 2D UNet to generate multi-scale image features and lift them to 3D space with TPVFormer [11]. After broadcasting TPV features, the voxel features are used for 3D semantic occupancy prediction and instance completion respectively. During inference, we adopt a mask-wise strategy to merge the results of two prediction heads.

number of interested semantic classes. Similar to [7], panoptic 3D scene reconstruction is to further predict instance id for each voxel belonging to foreground categories.

Our architecture, PanoSSC, shown in Fig. 2, solves the above tasks given only a single RGB image. The architecture starts from an arbitrary image backbone, and then a view transformation module, TPVFormer [11] in our implementation, to lift image features to 3D space. After that, we broadcast each TPV feature along the orthogonal direction and add them to obtain voxel feature. Along with a lightweight MLP-based semantic occupancy head, these voxel features are passed through a novel 3D mask decoder (Sec. 3.2) to improve the completion performance of the foreground instances. Under our training strategy (Sec. 3.3), these two prediction heads are able to boost each other. Inspired by Panoptic SegFormer [22], we employ a mask-wise strategy (Sec. 3.4) to merge predicted 3D masks from the final mask decoder layer with the background results from semantic occupancy head to obtain occupancy, semantics and instance ids for 3D voxelized scene.

**2D-3D encoder.** For fair comparisons with monocular pioneering work [2] on semantic occupancy prediction task, we employ the 2D UNet based on the pretrained EfficientNet-B7 [37] to generate multi-scale feature maps, of which the resolutions are 1/8, 1/16 compared to the input image. Then we use linear layers to convert the feature

dimension to 96 and send them to TPVFormer [11]. We follow the settings in [11] to stack 3 hybrid-cross-attention block (HCAB) blocks and 2 hybrid-attention block (HAB) blocks to form TPVFormer and set the number of queries on TPV planes to be  $128 \times 128$ ,  $16 \times 128$ ,  $128 \times 16$ . Each query encodes features of pillar region above the grid cell belonging to one of the TPV planes.

**Semantic occupancy head.** To obtain full-scale voxel features of size  $H \times W \times D \times C$  for fine-grained segmentation, we perform bilinear interpolation on the TPV features, and then broadcast each plane along the orthogonal direction and add them together. After that, the voxel features are fed into an MLP-based semantic occupancy head to predict their semantic labels, which consists of only two linear layers and an intermediate activation layer.

### 3.2. 3D mask decoder

To improve the reconstruction and segmentation quality of foreground instances, we also feed the voxel features into an instance completion head to conduct instance-aware semantic occupancy prediction. We propose a transformer-based 3D mask decoder as the instance completion head to predict categories and 3D masks from given queries, as shown in Fig. 3. We initialize  $N$  learnable reference points with uniform distribution from 0 to 1 in 3D space and involve positional encoding [40]. Then they are passed

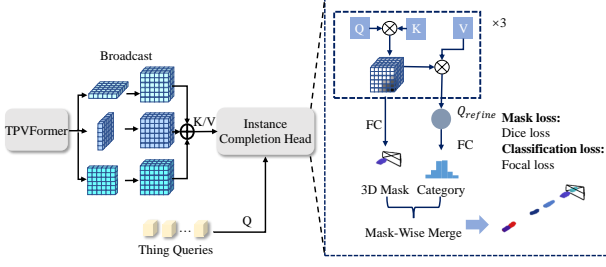


Figure 3. 3D mask decoder. We input the voxel features from TPVFormer [11] and the initialized thing queries into the transformer-based 3D mask decoder, which can generate 3D instance masks from attention maps and probabilities over all foreground categories from refined queries.

through an MLP consisting of two linear layers to generate the initial thing queries  $Q$ . The keys  $K$  and values  $V$  are projected from the voxel features. Specifically, due to computational cost constraints, TPV features are down-sampled by two convolution layers and an average pooling layer, and then broadcast to obtain 3D voxel features of size  $H/4 \times W/4 \times D/4 \times 256(C)$ .

3D mask decoder is stacked by multiple transformer layers, and each layer can generate attention maps  $A \in \mathbb{R}^{N \times h \times (\frac{H}{4} \times \frac{W}{4} \times \frac{D}{4})}$  and refined queries  $Q_{refined} \in \mathbb{R}^{N \times 256}$ , where  $h$  is the number of attention heads. This process can be formulated as:

$$A = \frac{QK^T}{\sqrt{d_k}} \quad (1)$$

$$Q_{refined} = \text{softmax}(A) \cdot V \quad (2)$$

where  $d_k$  is the dimension of  $Q$  and  $K$ . We use  $N = 300$ ,  $h = 8$  and stack 3 layers.

For  $Q_{refined}$  from each layer, a FC layer is used to directly predict probabilities over all foreground categories. At the same time, we use a linear layer to fuse the attention maps of multiple attention heads to obtain 3D masks  $M \in \mathbb{R}^{N \times (\frac{H}{4} \times \frac{W}{4} \times \frac{D}{4})}$ .

### 3.3. Training strategy

PanoSSC includes the multi-task learning from both semantic occupancy head and instance completion head. In multi-task learning, a common approach is to perform a weighted linear sum of the losses for each task [12]. But model performance heavily relies on weight selection. To get better results, we train our network in a fine-tuning two-stage manner.

At the first stage, we only train the network without instance completion head, which only consists of 2D UNet, TPVFormer and semantic occupancy head. We consider the semantic occupancy prediction task as a pre-training step. At this stage, in addition to the most commonly used

weighted cross-entropy loss  $\mathcal{L}_{ce}$  for semantic occupancy prediction, we also use the scene-class affinity loss  $\mathcal{L}_{scal}^{sem}$ ,  $\mathcal{L}_{scal}^{geo}$  and frustum proportion loss  $\mathcal{L}_{fp}$  proposed in [2] to optimize the global and local performance on this task. So the loss function at the first stage writes:

$$\mathcal{L}_{seg} = \mathcal{L}_{ce} + \mathcal{L}_{scal}^{sem} + \mathcal{L}_{scal}^{geo} + \mathcal{L}_{fp}. \quad (3)$$

Instance completion head can generate a fixed-size prediction set. Similar to transformer-based works [3, 22], we use Hungarian algorithm [15] to obtain the best bipartite matching between the prediction set and the ground truth set. The matching cost is the sum of classification cost and mask cost (classification loss  $\mathcal{L}_{cls}$  and mask loss  $\mathcal{L}_{mask}$ ). The loss for instance completion head is defined as:

$$\mathcal{L}_{inst} = \sum_i^{D_m} (\lambda_{cls} \mathcal{L}_{cls}^i + \lambda_{mask} \mathcal{L}_{mask}^i), \quad (4)$$

where  $D_m$  is the number of layers in 3D mask decoder,  $\lambda_{cls}$  and  $\lambda_{mask}$  are the weights. We employ focal loss [23] as classification loss  $\mathcal{L}_{cls}$  and dice loss [29] as mask loss  $\mathcal{L}_{mask}$ . In practice, we use  $D_m = 3$ ,  $\lambda_{cls} = 1$ ,  $\lambda_{mask} = 2$ .

At the second stage, we add instance completion head and reduce the learning rate of the rest of the network for joint training. The loss function at the second stage writes:

$$\mathcal{L} = \mathcal{L}_{seg} + \mathcal{L}_{inst}. \quad (5)$$

### 3.4. Mask-wise merging inference

This stage further refines the reconstruction quality of the foreground instances. We design a mask-wise merging strategy for 3D masks. During inference, it only takes the background prediction results of semantic occupancy head, and sets the voxels which belong to the foreground categories to empty. Then 3D masks from the instance completion head are merged one by one into the semantic occupancy prediction result. Since each mask represents a foreground instance, a unique id can be assigned. So PanoSSC can address the panoptic 3D scene reconstruction task.

Similar to [22], we calculate the confidence scores of 3D masks to determine the category and id of the overlap region. These scores consist of classification probabilities and mask quality scores. The score of  $i$ -th prediction writes:

$$s_i = p_i^\alpha \times \left( \frac{\sum m_i[h, w, d] \llbracket m_i[h, w, d] > 0.25 \rrbracket}{\sum \llbracket m_i[h, w, d] > 0.25 \rrbracket} \right)^\beta, \quad (6)$$

where  $\llbracket \cdot \rrbracket$  is the Iverson bracket,  $p_i$  is the maximum classification probability of  $i$ -th result,  $m_i[h, w, d]$  is the mask logit at voxel  $[h, w, d]$ ,  $\alpha, \beta$  are employed to balance the weight of classification probability and mask quality. In practice, we use  $\alpha = \frac{1}{3}$ ,  $\beta = 1$ . Note that since the resolution of 3D masks generated by the instance completion head is



---

**Algorithm 1** Mask-Wise Merging.

---

**Input:** background semantic result  $SemResult \in \mathbb{R}^{H \times W \times D}$ , the field of view of the image  $FOV \in \mathbb{R}^{H \times W \times D}$ , instance id result  $IdResult \in \mathbb{R}^{H \times W \times D}$ , categories  $c \in \mathbb{R}^N$ , scores  $s \in \mathbb{R}^N$ , masks  $m \in \mathbb{R}^{N \times H \times W \times D}$ .

**Output:** semantic result  $SemResult$ , instance id result  $IdResult$ .

```
1: Initialize:  $IdResult \leftarrow 0, id \leftarrow 1$ 
2: Sort results in descending order of score:  $order$ 
3: for  $i$  in  $order$  do
4:   if  $s[i] > t_q$  then
5:      $m_i \leftarrow (m[i] > 0.25) \& (SemResult = 0)$ 
6:     if  $\frac{m_i}{m[i] > 0.25} > t_{overlap}$  and  $\frac{m_i \& FOV}{m[i] > 0.25} > t_{fov}$  then
7:        $SemResult[m_i] \leftarrow c[i]$ 
8:        $IdResult[m_i] \leftarrow id$ 
9:        $id \leftarrow id + 1$ 
10:    end if
11:  end if
12: end for
```

---

$H/4 \times W/4 \times D/4$ , we perform trilinear interpolation to obtain full-scale masks, and then the masks are binarized with a threshold of 0.25.

Algorithm 1 illustrates our mask-wise merging strategy. It takes predicted categories  $c$ , confidence scores  $s$  and 3D masks  $m$  as input. These prediction results are arranged in descending order of confidence scores. In addition, the field of view of the image  $FOV$  is also input, in which the inside voxels are 1 and the outside voxels are 0. We set all voxels belonging to the foreground categories in the result from semantic occupancy head to 0 as the initial value of  $SemResult$ . And instance id result  $IdResult$  is initialized by zeros.

We merge masks into the final result in order and discard all masks with confidence scores below  $t_q$ . Then, we take the intersection of the current binarized mask and the empty voxels in  $SemResult$  to obtain non-overlap part  $m_i$  of the mask. If the proportion of  $m_i$  to the origin mask is lower than  $t_{overlap}$ , it is considered that there is a overlap conflict and the mask need to be discarded. Due to the extremely low prediction accuracy of instances outside the FOV, only masks that are mostly within  $FOV$  (above  $t_{fov}$ ) will be kept. Finally, the category label and instance id of each mask are assigned to  $SemResult$  and  $IdResult$  for panoptic 3D scene reconstruction. In practice, we use  $t_q = 0.2$ ,  $t_{overlap} = 0.5$ ,  $t_{fov} = 0.5$ .

## 4. Experiments

We evaluate PanoSSC on the densely annotated autonomous driving dataset SemanticKITTI [1]. In addition

to the SSC task, we propose the outdoor panoptic 3D scene reconstruction task and corresponding metrics (Sec. 4.1) based on this dataset. We provide our performance on two tasks (Sec. 4.2) and conduct ablation studies (Sec. 4.3).

### 4.1. Experimental setup

**Dataset.** The SSC task of SemanticKITTI [1] focuses on the volume of 51.2m ahead of the car, 25.6m to each side and 6.4m in height, and discretize it into  $256 \times 256 \times 32$  voxels. The voxels are labelled with 21 classes (19 semantics, 1 free and 1 unknown). Similar to previous work [2], we left crop RGB images of cam2 to  $1220 \times 370$ . We use the official 3834/815 train/val splits. To train and evaluate our network, we perform Euclidean clustering on the ground truth of train set and validation set to distinguish different instances. Notice that the dense semantic labels are obtained by the rigid registration of continuous frames [33], so moving objects (e.g. moving people) inevitably produce traces, which is an imperfection of SemanticKITTI. We filter out these traces when clustering. As shown in the supplementary material, by setting the clustering parameters reasonably, we can obtain unique ids for different instances.

**Training setup.** As mentioned in Sec. 3.3, we train our network in a two-stage manner. We first jointly pretrain 2D UNet, TPVFormer and semantic occupancy head on 4 RTX 3090 GPUs with an AdamW [26] optimizer using a batch size of 4, learning rate  $2e-4$  and a weight decay of 0.01 for 10 epochs. At the second stage, instance completion head is joined for joint training for another 10 epochs. With other settings unchanged, the learning rate is  $1e-4$  for instance completion head and  $1e-5$  for other parts.

**Metrics.** For semantic scene completion, we follow common practices to employ the intersection over union (IoU) of occupied voxels, regardless of their semantic labels, and the mean IoU (mIoU) of 19 semantic classes.

Similar to panoptic 3D scene reconstruction for indoor scenes [7], we calculate the average of panoptic reconstruction quality (PRQ) of different categories, where  $PRQ^c$  for the category  $c$  can be written as:

$$PRQ^c = \frac{\sum_{(h,w,d) \in TP^c} IoU(h,w,d)}{|TP^c| + \frac{1}{2}|FP^c| + \frac{1}{2}|FN^c|}, \quad (7)$$

where TP, FP and FN are the number of matched pairs of segments, unmatched predicted segments and unmatched ground-truth segments, respectively. Specifically, predicted and ground-truth segments are matched by a greedy search for the maximum IoU, and the match is considered successful if the voxelized IoU  $\geq 20\%$ . We evaluate PRQ of four categories: car, truck, other vehicle and road in SemanticKITTI. For the foreground categories, a segments is the voxels belonging to the same instance id, while all voxels belonging to the road category are a particular background segment. Consistent with the SSC task, we evaluate

Method	IoU (%)	mIoU (%)	Road (15.30%)	Parking (1.12%)	Sidewalk (11.13%)	Other-ground (0.56%)	Building (14.10%)	Fence (3.90%)	Vegetation (39.30%)	Terrain (9.17%)	Car (3.92%)	Bicycle (0.03%)	Motorcycle (0.03%)	Truck (0.16%)	Other-vehicle (0.20%)	Person (0.07%)	Bicyclist (0.07%)	Motorcyclist (0.05%)	Pole (0.29%)	Traffic-sign (0.08%)	Trunk (0.51%)	
LMSCNet <sup>rgb</sup> [34]*	28.61	6.70	40.68	4.38	18.22	0.00	10.31	1.21	13.66	20.54	18.33	0.00	0.00	0.00	0.00	0.00	0.00	0.00	0.00	0.00	0.00	0.02
3DSketch <sup>rgb</sup> [4]*	33.30	7.50	41.32	0.00	21.63	0.00	<u>14.81</u>	0.73	<b>19.09</b>	26.40	18.59	0.00	0.00	0.00	0.00	0.00	0.00	0.00	0.00	0.00	0.00	0.00
AICNet <sup>rgb</sup> [18]*	29.59	8.31	43.55	11.97	20.55	0.07	12.94	2.52	15.37	<u>28.71</u>	14.71	0.00	0.00	4.53	0.00	0.00	0.00	0.00	0.06	0.00	<u>2.90</u>	
JS3CNet <sup>rgb</sup> [46]*	<b>38.98</b>	10.31	50.49	11.94	23.74	0.07	<b>15.03</b>	3.94	<u>18.11</u>	<u>26.86</u>	<b>24.65</b>	0.00	0.00	4.41	6.15	0.67	<u>0.27</u>	0.00	3.77	1.45	<b>4.33</b>	
MonoScene [2]**	<u>36.87</u>	<b>11.27</b>	<u>55.92</u>	<u>14.55</u>	<b>26.51</b>	<b>1.55</b>	13.47	<b>6.66</b>	17.98	<b>29.90</b>	<u>23.34</u>	<u>0.24</u>	<b>0.74</b>	<u>9.05</u>	2.59	<b>1.96</b>	<b>1.08</b>	0.00	<b>3.84</b>	<b>2.40</b>	2.41	
PanoSSC (ours)	<u>34.94</u>	<u>11.22</u>	<b>56.36</b>	<b>17.76</b>	<u>26.40</u>	<u>0.88</u>	14.26	<u>5.72</u>	16.69	28.05	19.63	<b>0.63</b>	<u>0.36</u>	<b>14.79</b>	<b>6.22</b>	<u>0.87</u>	0.00	0.00	1.94	0.70	1.83	

Table 1. Semantic scene completion results on SemanticKITTI validation set. (\* represents that the results are reported on [2]. \*\* represents the reproduced result using the official code and checkpoint.)

	PRQ	RSQ	RRQ	PRQ	RSQ	RRQ	PRQ	RSQ	RRQ			
				things				stuff				
MonoScene [2] + EC	19.33	37.83	38.26	6.51	30.90	18.15	57.79	58.63	<b>98.58</b>			
TPVFormer [11] + EC	18.94	32.18	36.40	6.39	23.50	16.12	56.59	58.20	97.22			
PanoSSC (ours)	<b>22.93</b>	<b>39.51</b>	<b>49.43</b>	<b>11.27</b>	<b>33.02</b>	<b>33.20</b>	<b>57.90</b>	<b>59.00</b>	98.13			

Table 2. Panoptic 3D scene reconstruction results on SemanticKITTI validation set. (EC: Euclidean clustering.)

		MonoScene [2] +EC	TPVFormer [11] +EC	PanoSSC (ours)
Car	PRQ	14.73	<b>16.95</b>	16.38
	RSQ	41.03	<b>41.68</b>	35.65
	RRQ	35.90	40.68	<b>45.95</b>
Truck	PRQ	4.06	0.00	<b>13.26</b>
	RSQ	25.89	0.00	<b>33.34</b>
	RRQ	15.67	0.00	<b>39.78</b>
Other-vehicle	PRQ	0.74	2.21	<b>4.17</b>
	RSQ	25.77	28.82	<b>30.07</b>
	RRQ	2.88	7.68	<b>13.87</b>
Road	PRQ	57.79	56.59	<b>57.90</b>
	RSQ	58.63	58.20	<b>59.00</b>
	RRQ	98.58	97.22	<b>98.13</b>

Table 3. Panoptic 3D scene reconstruction results for each category on SemanticKITTI validation set. (EC: Euclidean clustering.)

panoptic reconstruction at a voxel resolution of 0.2m and ignore unknown voxels. In addition, the  $PRQ^c$  can be regarded as the product of reconstructed segmentation quality  $RSQ^c$  and reconstructed recognition quality  $RRQ^c$ :

$$PRQ^c = RSQ^c \times RRQ^c = \frac{\sum_{(h,w,d) \in TP} \text{IoU}(h,w,d)}{|TP^c|} \times \frac{|TP^c|}{|TP^c| + \frac{1}{2}|FP^c| + \frac{1}{2}|FN^c|}. \quad (8)$$

We also report the average of RSQ and RRQ.

## 4.2. Performance

**Baselines.** We use the state-of-the-art method MonoScene [2] as a baseline for semantic scene completion and further cluster the semantic results with Euclidean clustering as the baseline for panoptic 3D scene reconstruction.

**Semantic scene completion.** Tab. 1 reports the performance of PanoSSC and baselines on SemanticKITTI. Our network achieves performance on par with the state-of-the-art monocular work on the main metric mIoU (11.22 vs 11.27). And the parameter number of PanoSSC is less (137M vs 149M). Besides, our network helps distinguish similar categories and significantly improve the reconstruction of trucks (+5.74) and other vehicles (+3.63). But it is undeniable that PanoSSC’s reconstruction of moving objects need to be improved (in SemanticKITTI, for categories like person, there are far more moving objects than stationary ones). We attribute this partly to the imperfection of ground truth in SemanticKITTI mentioned above, that is, moving objects produce traces and do not have the correct shape. Our network performs SSC in the form of reconstructing each instance, which is more susceptible to confusion caused by this imperfection. In addition, PanoSSC infers a global 3D voxel mask for each instance, so the reconstruction accuracy of small object categories also needs improvement.

**Panoptic 3D scene reconstruction.** Tab. 2 reports results of panoptic 3D scene reconstruction. Our network evidently outperforms clustering the output of SSC methods.

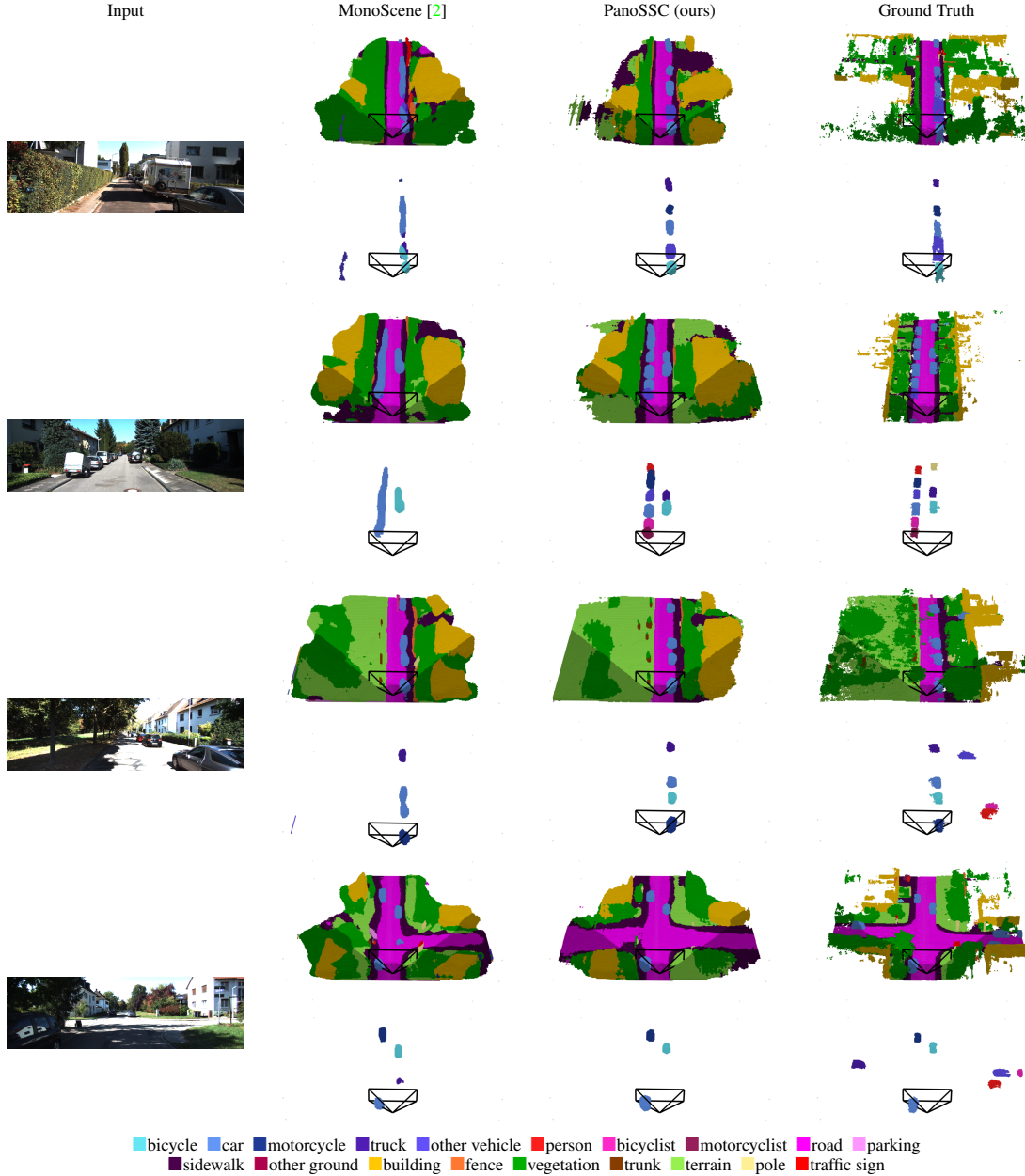


Figure 4. Visualization on the SemanticKITTI [1] validation set. Each pair of rows shows the results of semantic scene completion (upper) and 3D instance completion for vehicle (lower). Different color bars represent different categories on the SSC task, while colors indicate different instance for 3D instance completion. The darker voxels are outside FOV of the image. Compared to MonoScene [2], our PanoSSC can better capture the road layout (row 7) and estimate the shape of vehicles (rows 1 – 6), especially when they are close. It can also better distinguish similar categories, *e.g.* car and truck (rows 1 – 4).

Compared with MonoScene, panoptic reconstruction quality (PRQ) of PanoSSC is higher (+3.60), especially for the foreground categories (+4.76). Tab. 3 reports the results for each category. Compared with performing Euclidean clustering on the output of semantic occupancy head followed by TPVFormer, adding instance completion head greatly improves PRQ of truck and other-vehicle (+13.26,+1.96).

That is, our network can more accurately distinguish these three similar categories: car, truck and other-vehicle.

**Qualitative results.** Panoptic 3D scene reconstruction involves semantic completion for background categories and instance completion for foreground categories. Fig. 4 shows the SSC output (upper of each pair of rows) and the instance completion results (lower of each pair of rows).

	mIoU	IoU
Ours w/o instance completion head	10.59	34.95
Output of semantic occupancy head of ours	10.77	<b>35.21</b>
Ours (after merging)	<b>11.22</b>	34.94

Table 4. Effect of instance completion head on semantic scene completion in multi-task learning.

	PRQ	RSQ	RRQ	mIoU
	things (car,truck,other-vehicle)			
Ours w/o semantic occupancy head	5.59	21.38	28.26	6.34
Ours	11.27	33.02	33.20	13.55

Table 5. Effect of semantic occupancy head on instance completion in multi-task learning.

MonoScene tends to predict the empty voxels in the vehicle interval as vehicle on the SSC task. Therefore, when simply clustering the output of SSC, it is impossible to assign unique ids to multiple vehicles in the strip (rows 2,4). While PanoSSC can obtain the 3D mask of each instance and merge them, which can better distinguish the close instances and estimate their shape (rows 1,3,5). Besides, since other existing SSC methods use a per-voxel classification formulation, there is a mixture of voxels belonging to the similar categories during semantic occupancy prediction. That is, there are few truck voxels in the region that is mostly predicted to be car voxels (row 1). We adopt mask-wise classification and discard some masks according to overlap conflicts during inference, which can suppress these unreasonable results. In addition, PanoSSC can also better reconstruct road layout (row 7) and distinguish similar categories, *e.g.* car and truck (rows 1,3). Note that none of the existing monocular works can reconstruct the completely occluded objects in the scene well (rows 6,8). More qualitative results are presented in the supplementary material.

### 4.3. Ablation studies

**Multi-task learning.** Inspired by works in 2D domain, our network includes semantic occupancy head and instance completion head for multi-task learning. To prove that these two heads can boost each other, we conduct ablation studies. In Tab. 4, we report the SSC results of our network, the network without instance completion head, and the semantic occupancy head after joint training. It is shown that even without merging the output of instance completion head, joining this head for training can improve SSC performance (mIoU+0.18, IoU+0.26). Merging the output of instance completion head can further boost the main metric of the SSC task (+0.45). Tab. 5 shows that ablating semantic occupancy head also impairs the performance of instance completion. We conjecture that this mutual promotion comes

	mIoU	IoU	PRQ	RSQ	RRQ
$\lambda_{cls} : \lambda_{mask} = 2 : 1$	10.97	34.67	21.37	39.34	44.97
$\lambda_{cls} : \lambda_{mask} = 1 : 1$	11.03	34.78	21.54	39.51	45.00
$\lambda_{cls} : \lambda_{mask} = 1 : 2$ (ours)	<b>11.22</b>	<b>34.95</b>	<b>22.93</b>	<b>39.51</b>	<b>49.43</b>

Table 6. Effect of loss weights in instance completion head.

Layer	PRQ	RSQ	RRQ
1	21.13	39.44	44.18
2	21.78	38.97	46.38
3	22.93	39.52	49.43

Table 7. Panoptic 3D scene reconstruction results for each layer in instance completion head.

from the improvement of generalization by sharing domain information between related tasks.

**Losses.** The loss of instance completion head in Eq. (4) consists of classification loss and mask loss, and we need to balance these two losses. We find that classification loss converges slightly faster than mask loss. Tab. 6 shows that appropriately reducing the weight of classification loss is beneficial to the network to obtain good results. We speculate that this is because classification is easier than estimation of shape and position for mask decoder.

**Mask decoder.** As mentioned in Sec. 3.2, instance completion head is stacked by multiple transformer layers and each layer can generate a set of classification probabilities and 3D masks. Tab. 7 reports the results of each layer in instance completion head. As the number of layers increases, the reconstruction quality of the output improves. Considering the parameter amount and inference speed of the network, our PanoSSC only stacks 3 layers.

## 5. Conclusion

In this paper, we proposed a novel voxelized scene understanding method, coined PanoSSC, which can tackle semantic occupancy prediction and panoptic 3D scene reconstruction on outdoor. Our method joins semantic occupancy head and instance completion head for joint training to achieve mutual promotion. On the SemanticKITTI dataset, we perform on par with the state-of-the-art monocular method on semantic occupancy prediction task. And to our best knowledge, PanoSSC is the first vision-only panoptic 3D scene reconstruction method on outdoor and achieves good results. We hope that our work can advance the research on more comprehensive scene understanding for autonomous driving.

## References

- [1] Jens Behley, Martin Garbade, Andres Milioto, Jan Quenzel, Sven Behnke, Cyrill Stachniss, and Jürgen Gall. Se-



- mantickitti: A dataset for semantic scene understanding of lidar sequences. In *2019 IEEE/CVF International Conference on Computer Vision (ICCV)*, pages 9296–9306, 2019. 2, 5, 7
- [2] Anh-Quan Cao and Raoul de Charette. Monoscene: Monocular 3d semantic scene completion. In *Proceedings of the IEEE/CVF Conference on Computer Vision and Pattern Recognition*, pages 3991–4001, 2022. 2, 3, 4, 5, 6, 7
- [3] Nicolas Carion, Francisco Massa, Gabriel Synnaeve, Nicolas Usunier, Alexander Kirillov, and Sergey Zagoruyko. End-to-end object detection with transformers. In *Computer Vision—ECCV 2020: 16th European Conference, Glasgow, UK, August 23–28, 2020, Proceedings, Part I 16*, pages 213–229. Springer, 2020. 2, 4
- [4] Xiaokang Chen, Kwan-Yee Lin, Chen Qian, Gang Zeng, and Hongsheng Li. 3d sketch-aware semantic scene completion via semi-supervised structure prior. In *Proceedings of the IEEE/CVF Conference on Computer Vision and Pattern Recognition (CVPR)*, 2020. 2, 6
- [5] Bowen Cheng, Alex Schwing, and Alexander Kirillov. Pixel classification is not all you need for semantic segmentation. *Advances in Neural Information Processing Systems*, 34:17864–17875, 2021. 2
- [6] Ran Cheng, Christopher Agia, Yuan Ren, Xinhai Li, and Liu Bingbing. S3cnet: A sparse semantic scene completion network for lidar point clouds. *arXiv preprint arXiv:2012.09242*, 2020. 2
- [7] Manuel Dahnert, Ji Hou, Matthias Nießner, and Angela Dai. Panoptic 3d scene reconstruction from a single rgb image. *Advances in Neural Information Processing Systems*, 34: 8282–8293, 2021. 2, 3, 5
- [8] Martin Garbade, Yueh-Tung Chen, Johann Sawatzky, and Juergen Gall. Two stream 3d semantic scene completion. In *Proceedings of the IEEE/CVF Conference on Computer Vision and Pattern Recognition Workshops*, pages 0–0, 2019. 2
- [9] Bharath Hariharan, Pablo Arbeláez, Ross Girshick, and Jitendra Malik. Simultaneous detection and segmentation. In *Computer Vision—ECCV 2014: 13th European Conference, Zurich, Switzerland, September 6–12, 2014, Proceedings, Part VII 13*, pages 297–312. Springer, 2014. 2
- [10] Kaiming He, Georgia Gkioxari, Piotr Dollár, and Ross Girshick. Mask r-cnn. In *Proceedings of the IEEE international conference on computer vision*, pages 2961–2969, 2017. 2
- [11] Yuanhui Huang, Wenzhao Zheng, Yunpeng Zhang, Jie Zhou, and Jiwen Lu. Tri-perspective view for vision-based 3d semantic occupancy prediction. In *Proceedings of the IEEE/CVF Conference on Computer Vision and Pattern Recognition*, pages 9223–9232, 2023. 1, 2, 3, 4, 6
- [12] Alex Kendall, Yarin Gal, and Roberto Cipolla. Multi-task learning using uncertainty to weigh losses for scene geometry and semantics. In *Proceedings of the IEEE conference on computer vision and pattern recognition*, pages 7482–7491, 2018. 2, 4
- [13] Alexander Kirillov, Ross Girshick, Kaiming He, and Piotr Dollár. Panoptic feature pyramid networks. In *Proceedings of the IEEE/CVF conference on computer vision and pattern recognition*, pages 6399–6408, 2019. 2
- [14] Alexander Kirillov, Kaiming He, Ross Girshick, Carsten Rother, and Piotr Dollár. Panoptic segmentation. In *Proceedings of the IEEE/CVF Conference on Computer Vision and Pattern Recognition*, pages 9404–9413, 2019. 2
- [15] H. W. Kuhn. The hungarian method for the assignment problem. *Naval Research Logistics Quarterly*, 2(1-2):83–97, 1995. 4
- [16] Abhijit Kundu, Kyle Genova, Xiaoqi Yin, Alireza Fathi, Caroline Pantofaru, Leonidas J Guibas, Andrea Tagliasacchi, Frank Dellaert, and Thomas Funkhouser. Panoptic neural fields: A semantic object-aware neural scene representation. In *Proceedings of the IEEE/CVF Conference on Computer Vision and Pattern Recognition*, pages 12871–12881, 2022. 2
- [17] Jie Li, Yu Liu, Dong Gong, Qinfeng Shi, Xia Yuan, Chunxia Zhao, and Ian Reid. Rgb-d based dimensional decomposition residual network for 3d semantic scene completion. In *Proceedings of the IEEE/CVF Conference on Computer Vision and Pattern Recognition*, pages 7693–7702, 2019. 2
- [18] Jie Li, Kai Han, Peng Wang, Yu Liu, and Xia Yuan. Anisotropic convolutional networks for 3d semantic scene completion. In *Proceedings of the IEEE/CVF Conference on Computer Vision and Pattern Recognition (CVPR)*, 2020. 2, 6
- [19] Yiming Li, Sihang Li, Xinhao Liu, Moonjun Gong, Kenan Li, Nuo Chen, Zijun Wang, Zhiheng Li, Tao Jiang, Fisher Yu, et al. Sscbench: A large-scale 3d semantic scene completion benchmark for autonomous driving. *arXiv preprint arXiv:2306.09001*, 2023. 1
- [20] Yiming Li, Zhiding Yu, Christopher Choy, Chaowei Xiao, Jose M Alvarez, Sanja Fidler, Chen Feng, and Anima Anandkumar. Voxformer: Sparse voxel transformer for camera-based 3d semantic scene completion. In *Proceedings of the IEEE/CVF Conference on Computer Vision and Pattern Recognition*, pages 9087–9098, 2023. 2
- [21] Zhiqi Li, Wenhai Wang, Hongyang Li, Enze Xie, Chonghao Sima, Tong Lu, Yu Qiao, and Jifeng Dai. Bevformer: Learning bird’s-eye-view representation from multi-camera images via spatiotemporal transformers. In *Computer Vision—ECCV 2022: 17th European Conference, Tel Aviv, Israel, October 23–27, 2022, Proceedings, Part IX*, pages 1–18. Springer, 2022. 2
- [22] Zhiqi Li, Wenhai Wang, Enze Xie, Zhiding Yu, Anima Anandkumar, Jose M Alvarez, Ping Luo, and Tong Lu. Panoptic segformer: Delving deeper into panoptic segmentation with transformers. In *Proceedings of the IEEE/CVF Conference on Computer Vision and Pattern Recognition*, pages 1280–1289, 2022. 2, 3, 4, 1
- [23] Tsung-Yi Lin, Priya Goyal, Ross Girshick, Kaiming He, and Piotr Dollár. Focal loss for dense object detection. In *Proceedings of the IEEE International Conference on Computer Vision (ICCV)*, 2017. 4
- [24] Yingfei Liu, Junjie Yan, Fan Jia, Shuailin Li, Qi Gao, Tiancai Wang, Xiangyu Zhang, and Jian Sun. Petrv2: A unified framework for 3d perception from multi-camera images. *arXiv preprint arXiv:2206.01256*, 2022. 2
- [25] Jonathan Long, Evan Shelhamer, and Trevor Darrell. Fully convolutional networks for semantic segmentation. In *Pro-*

- ceedings of the IEEE conference on computer vision and pattern recognition, pages 3431–3440, 2015. 2
- [26] Ilya Loshchilov and Frank Hutter. Decoupled weight decay regularization. In *International Conference on Learning Representations*, 2018. 5
- [27] Jiageng Mao, Shaoshuai Shi, Xiaogang Wang, and Hongsheng Li. 3d object detection for autonomous driving: a review and new outlooks. *arXiv preprint arXiv:2206.09474*, 2022. 1
- [28] Ruihang Miao, Weizhou Liu, Mingrui Chen, Zheng Gong, Weixin Xu, Chen Hu, and Shuchang Zhou. Occdepth: A depth-aware method for 3d semantic scene completion. *arXiv preprint arXiv:2302.13540*, 2023. 2
- [29] Fausto Milletari, Nassir Navab, and Seyed-Ahmad Ahmadi. V-net: Fully convolutional neural networks for volumetric medical image segmentation. In *2016 Fourth International Conference on 3D Vision (3DV)*, pages 565–571, 2016. 4
- [30] Mingjie Pan, Li Liu, Jiaming Liu, Peixiang Huang, Longlong Wang, Shanghang Zhang, Shaoqing Xu, Zhiyi Lai, and Kuiyuan Yang. Uniocc: Unifying vision-centric 3d occupancy prediction with geometric and semantic rendering. *arXiv preprint arXiv:2306.09117*, 2023. 1
- [31] Jonah Philion and Sanja Fidler. Lift, splat, shoot: Encoding images from arbitrary camera rigs by implicitly unprojecting to 3d. In *Computer Vision—ECCV 2020: 16th European Conference, Glasgow, UK, August 23–28, 2020, Proceedings, Part XIV 16*, pages 194–210. Springer, 2020. 2
- [32] Christoph B. Rist, David Emmerichs, Markus Enzweiler, and Dariu M. Gavrilă. Semantic scene completion using local deep implicit functions on lidar data. *IEEE Transactions on Pattern Analysis and Machine Intelligence*, 44(10):7205–7218, 2022. 2
- [33] Luis Roldao, Raoul De Charette, and Anne Verroust-Blondet. 3d semantic scene completion: A survey. *International Journal of Computer Vision*, 130(8):1978–2005, 2022. 5
- [34] Luis Roldão, Raoul de Charette, and Anne Verroust-Blondet. Lmscnet: Lightweight multiscale 3d semantic completion. In *2020 International Conference on 3D Vision (3DV)*, pages 111–119, 2020. 2, 6
- [35] Yining Shi, Kun Jiang, Jiushi Li, Junze Wen, Zelin Qian, Mengmeng Yang, Ke Wang, and Diange Yang. Grid-centric traffic scenario perception for autonomous driving: A comprehensive review. *arXiv preprint arXiv:2303.01212*, 2023. 1
- [36] Shuran Song, Fisher Yu, Andy Zeng, Angel X Chang, Manolis Savva, and Thomas Funkhouser. Semantic scene completion from a single depth image. In *Proceedings of the IEEE conference on computer vision and pattern recognition*, pages 1746–1754, 2017. 2
- [37] Mingxing Tan and Quoc Le. Efficientnet: Rethinking model scaling for convolutional neural networks. In *International conference on machine learning*, pages 6105–6114. PMLR, 2019. 3
- [38] Xiaoyu Tian, Tao Jiang, Longfei Yun, Yue Wang, Yilun Wang, and Hang Zhao. Occ3d: A large-scale 3d occupancy prediction benchmark for autonomous driving. *arXiv preprint arXiv:2304.14365*, 2023. 1
- [39] Wenwen Tong, Chonghao Sima, Tai Wang, Silei Wu, Hanming Deng, Li Chen, Yi Gu, Lewei Lu, Ping Luo, Dahua Lin, et al. Scene as occupancy. *arXiv preprint arXiv:2306.02851*, 2023. 1
- [40] Ashish Vaswani, Noam Shazeer, Niki Parmar, Jakob Uszkoreit, Llion Jones, Aidan N Gomez, Łukasz Kaiser, and Illia Polosukhin. Attention is all you need. *Advances in neural information processing systems*, 30, 2017. 3
- [41] Huiyu Wang, Yukun Zhu, Hartwig Adam, Alan Yuille, and Liang-Chieh Chen. Max-deeplab: End-to-end panoptic segmentation with mask transformers. In *Proceedings of the IEEE/CVF conference on computer vision and pattern recognition*, pages 5463–5474, 2021. 2
- [42] Xiaofeng Wang, Zheng Zhu, Wenbo Xu, Yunpeng Zhang, Yi Wei, Xu Chi, Yun Ye, Dalong Du, Jiwen Lu, and Xingang Wang. Openoccupancy: A large scale benchmark for surrounding semantic occupancy perception. *arXiv preprint arXiv:2303.03991*, 2023. 1
- [43] Yuqi Wang, Yuntao Chen, Xingyu Liao, Lue Fan, and Zhaoxiang Zhang. Panoocc: Unified occupancy representation for camera-based 3d panoptic segmentation. *arXiv preprint arXiv:2306.10013*, 2023. 1, 2
- [44] Joey Wilson, Jingyu Song, Yuewei Fu, Arthur Zhang, Andrew Capodieci, Paramsothy Jayakumar, Kira Barton, and Maani Ghaffari. Motionsc: Data set and network for real-time semantic mapping in dynamic environments. *IEEE Robotics and Automation Letters*, 7(3):8439–8446, 2022. 2
- [45] Shun-Cheng Wu, Keisuke Tateno, Nassir Navab, and Federico Tombari. Sefusion: Real-time incremental scene reconstruction with semantic completion. In *2020 International Conference on 3D Vision (3DV)*, pages 801–810. IEEE, 2020. 2
- [46] Xu Yan, Jiantao Gao, Jie Li, Ruimao Zhang, Zhen Li, Rui Huang, and Shuguang Cui. Sparse single sweep lidar point cloud segmentation via learning contextual shape priors from scene completion. In *Proceedings of the AAAI Conference on Artificial Intelligence*, pages 3101–3109, 2021. 2, 6
- [47] Dongqiangzi Ye, Zixiang Zhou, Weijia Chen, Yufei Xie, Yu Wang, Panqu Wang, and Hassan Foroosh. Lidarmultinet: Towards a unified multi-task network for lidar perception, 2023. 2
- [48] Jiahui Zhang, Hao Zhao, Anbang Yao, Yurong Chen, Li Zhang, and Hongen Liao. Efficient semantic scene completion network with spatial group convolution. In *Proceedings of the European Conference on Computer Vision (ECCV)*, pages 733–749, 2018. 2

# PanoSSC: Exploring Monocular Panoptic 3D Scene Reconstruction for Autonomous Driving

## Supplementary Material

### 6. 3D mask decoder

As described in [22], using a lightweight FC layer to generate masks from attention maps enables the attention module to learn where to focus guided by the ground truth mask. We extend the mask decoder in [22] to 3D segmentation and completion, and also use deep supervision, which means that attention maps of each layer are supervised by the ground truth 3D mask. Therefore, the attention module can focus on interested region as early as possible, which accelerating the learning and convergence of the model.

### 7. Dataset setup.

When training instance completion head, the 3D binary mask and the category label for each instance is required. While SemanticKITTI only provides ground-truth semantic labels without instance ids and moving objects inevitably produce traces. To train and evaluate our network, we perform Euclidean clustering on the ground truth and filter out those traces. In practice, we set the search radius of Euclidean clustering to be 2 voxels for vehicles and 3 voxels for other categories. The maximum number of voxels per cluster is 2000 for cars, 5000 for trucks and other-vehicles, and 1000 for people, bicyclists and motorcyclists. As shown in Fig. 5, we can obtain unique ids for different instances by setting the reasonable clustering parameters.

monly used in SSC methods, the mask-wise classification and merging strategy in PanoSSC can suppress these unreasonable results.

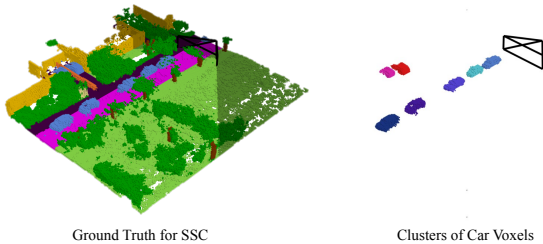


Figure 5. Instance ids obtained from Euclidean clustering on the ground truth for SSC.

### 8. Qualitative results

Fig. 6 shows additional qualitative results on SemanticKITTI validation set. Notice our network can better distinguish the close instances and estimate their shape. Fig. 7 provides zoom-in view of a mixture of voxels belonging to the car and truck categories. It can be clearly shown that compared with the per-voxel classification com-

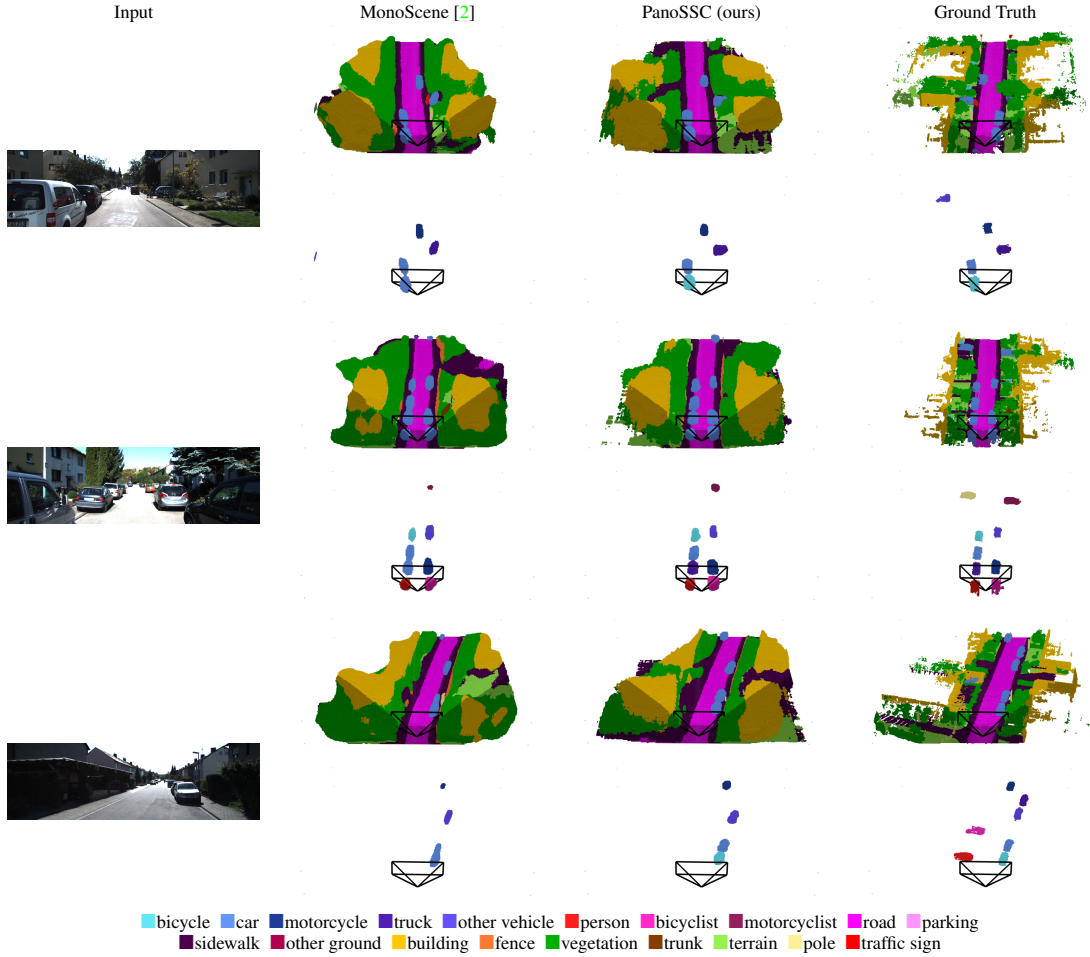


Figure 6. Additional qualitative results on the SemanticKITTI [1] validation set. Each pair of rows shows the results of semantic scene completion (upper) and 3D instance completion for vehicle (lower). Different color bars represent different categories in SSC task, while colors indicate different instance for 3D instance completion. The darker voxels are outside FOV of the image.

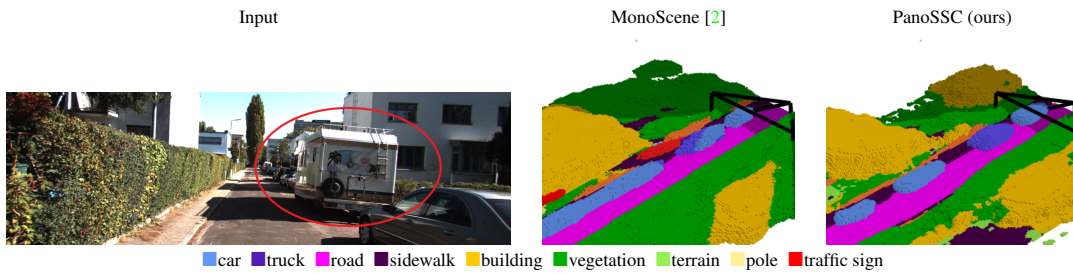


Figure 7. Zoom-in view of a mixture of voxels belonging to the similar categories during semantic occupancy prediction.